JCI insight

Monocyte glycolysis determines CD8+ T-cell functionality in human Chagas disease

Liliana María Sanmarco, … , Miriam Postan, Maria Pilar Aoki

JCI Insight. 2019. https://doi.org/10.1172/jci.insight.123490.

Research In-Press Preview Immunology Metabolism

Chagas disease is a life-long pathology resulting from *Trypanosoma cruzi* infection. It represents one of the most frequent causes of heart failure and sudden death in Latin America. Herein we provide evidence that aerobic glycolytic pathway activation in monocytes drives nitric oxide (NO) production, triggering tyrosine nitration (TN) on CD8 T cells and dysfunction in patients with chronic Chagas disease. Monocytes from patients exhibited higher frequency of hypoxia inducible factor (HIF)-1α and increased expression of its target genes/proteins. Non-classical monocytes are expanded in patients´ peripheral blood and represent an important source of NO. Monocytes entail CD8 T cell surface nitration since both the frequency of non-classical monocytes and that of NO-producing monocytes, positively correlated with the percentage of TN^+ lymphocytes. Inhibition of glycolysis in (in vitro) infected peripheral blood mononuclear cells decreased the inflammatory properties of monocytes/macrophages diminishing the frequency of IL-1β- and NO-producing cells. In agreement, glycolysis inhibition reduced the percentage of TN^+CD8 T cells improving their functionality. Altogether, these results clearly evidence that glycolysis governs oxidative stress on monocytes and modulates monocyte-T cell interplay in human chronic Chagas disease. Understanding the pathological immune mechanisms that sustains inflammatory environment in human pathology is key to design improved therapies.

Monocyte glycolysis determines CD8+ T-cell functionality in human Chagas disease

Liliana María Sanmarco [1, 2, 8], Natalia Eberhardt [1, 2], Gastón Bergero [1, 2], Luz Piedad Quebrada Palacio [3], Pamela Martino Adami [4], Laura Marina Visconti [5,6], Ángel Ramón Minguez [5], Yolanda Hernández-Vasquez [3], Eugenio Antonio Carrera Silva [7], Laura Morelli [4], Miriam Postan [3], Maria Pilar Aoki [1, 2] *.

1 Universidad Nacional de Córdoba, Facultad de Ciencias Químicas, Departamento de Bioquímica Clínica, Córdoba, Argentina.
2 Consejo Nacional de Investigaciones Científicas y Tecnológicas (CONICET), Centro de Investigaciones en Bioquímica Clínica e Inmunología (CIBICI), Córdoba, Argentina.
3 Instituto Nacional de Parasitología Dr. Mario Fatala Chabén, Buenos Aires, Argentina.
4 Laboratorio de Amiloidosis y Neurodegeneración, Fundación Instituto Leloir, Buenos Aires, Argentina; Instituto de Investigaciones Bioquímicas de Buenos Aires, Consejo Nacional de Investigaciones Científicas y Técnicas (CONICET), Buenos Aires, Argentina.
5 Hospital Nuestra Señora de la Misericordia, Córdoba, Argentina.
6 Universidad Nacional de Córdoba, Facultad de Ciencias Médicas, II Cátedra de Infectología, Córdoba, Argentina.
7 Laboratorio de Trombosis Experimental, Instituto de Medicina Experimental (IMEX), Academia Nacional de Medicina, Consejo Nacional de Investigaciones Científicas y Técnicas (CONICET), Buenos Aires, Argentina.
8 Ann Romney Center for Neurologic Diseases, Brigham and Women's Hospital. Harvard Medical School, Boston, MA, United States (current affiliation).

*Corresponding author: Maria Pilar Aoki
Address: Haya de la Torre and Medina Allende. Ciudad Universitaria. CP 5000. Córdoba. Argentina. Tel: +54-351-5353851 ext 3181. Fax: +54-351-4333048 ext 3177.
E-mail: paoki@fcq.unc.edu.ar

The authors have declared that no conflict of interest exists.

Abstract

Chagas disease is a life-long pathology resulting from *Trypanosoma cruzi* infection. It represents one of the most frequent causes of heart failure and sudden death in Latin America. Herein we provide evidence that aerobic glycolytic pathway activation in monocytes drives nitric oxide (NO) production, triggering tyrosine nitration (TN) on CD8 T cells and dysfunction in patients with chronic Chagas disease. Monocytes from patients exhibited higher frequency of hypoxia inducible factor (HIF)-1α and increased expression of its target genes/proteins. Non-classical monocytes are expanded in patients´ peripheral blood and represent an important source of NO. Monocytes entail CD8 T cell surface nitration since both the frequency of non-classical monocytes and that of NO-producing monocytes, positively correlated with the percentage of TN^+ lymphocytes. Inhibition of glycolysis in (in vitro) infected peripheral blood mononuclear cells decreased the inflammatory properties of monocytes/macrophages diminishing the frequency of IL-1β- and NO-producing cells. In agreement, glycolysis inhibition reduced the percentage of TN^+CD8 T cells improving their functionality. Altogether, these results clearly evidence that glycolysis governs oxidative stress on monocytes and modulates monocyte-T cell interplay in human chronic Chagas disease. Understanding the pathological immune mechanisms that sustains inflammatory environment in human pathology is key to design improved therapies.

Introduction

Monocytes are critical components not only of the innate immune system but also of adaptive immune response development. Based on the relative surface expression of LPS co-receptor CD14 and of FcγIII receptor CD16, they have been classified into three subtypes: “classical monocytes” ($CD14^{++}CD16^{-}$), “non-classical monocytes” ($CD14^{+}CD16^{++}$), and “intermediate monocytes” ($CD14^{++}CD16^{+}$) (1, 2). So far, however, there is poor understanding of the effector functions of each monocyte subset and numerous reports show contradictory results (3).

Under hypoxic or inflammatory conditions, monocytes activate transcriptional responses, which are governed by the transcription factor hypoxia-inducible factor (HIF)-1α. The accumulation of HIF-1α protein requires the metabolism of glucose into pyruvate that prevents the aerobic degradation of HIF-1α protein. HIF-1α-target genes include glucose transporters GLUT-1 and GLUT-3 (4-6). Glucose can be used throughout two integrated pathways, the first of which, the glycolytic pathway, involves the cytoplasmic conversion of glucose into pyruvate, with the consequent generation of 2 ATP molecules and, in anaerobic conditions, lactate. Extracellular ATP (eATP) and lactate activate HIF-1α (7, 8), thus resulting in a positive feedback. The second pathway, the tricarboxylic acid cycle, generates the reducing equivalents nicotinamide adenine dinucleotide (NADH) and flavin adenine dinucleotide (FADH2), which donate electrons to the electron transport chain to fuel oxidative phosphorylation (OXPHOS), the process by which 32 ATP molecules are generated in the mitochondria.

In inflammatory settings, the OXPHOS is inhibited by nitric oxide (NO) production in monocyte-derived inflammatory dendritic cells (moDC) in an autocrine manner. In the absence of active respiratory chain, sustained glycolytic metabolism is essential for moDC survival and function (9). Furthermore, NO production seems to be central in orchestrating HIF-1α responses by inducing its stabilization and transcriptional activation (10).

Chagas disease, a complex pathological condition resulting from *Trypanosoma cruzi* infection, has become one of the most frequent causes of heart failure, cardio-embolic stroke and sudden death in Latin America (11). The acute phase lasts 2 to 3 months and is characterized by detectable parasitemia and active parasite replication within target tissues. However, clinical symptoms are usually mild and non-specific and the vast majority of acute infections are never detected. During this phase, cell-mediated immunity controls parasite levels, but it is insufficient to completely clear the infection and most individuals remain infected for life. People who survive the acute phase enter a chronic asymptomatic phase (indeterminate stage), which is generally symptomless and may last from 10 to 30 years. Approximately 30% of patients in this period, also recognized as “silent”, may develop heart abnormalities (12) that could give rise to the cardiac form of chronic infection. Although anti-parasitic therapy is clearly recommended for acute Chagas disease, the treatment of patients in the chronic stage is controversial. This is largely due to a lack of large, randomized trials and incomplete understanding of pathological immune mechanisms developed during this stage. After decades of controversies, it is widely accepted nowadays that parasite persistence is a necessary and sufficient condition for the sustained inflammatory responses underlying the progression of cardiac lesions of chronic Chagas disease (13-18). Thus, one of the main challenges in understanding Chagas myocarditis immunopathology is to find out why, despite a robust immune response during the acute phase of the infection, the parasite is not completely eliminated, being able to sustain pathological inflammatory environment.

Cell-mediated immunity involves activation of phagocytes and of cytotoxic T-lymphocytes (CTLs). In this sense, we have recently reported increased IL-1β plasma levels concomitant with enhanced frequency of NO-producing leukocytes and the surface nitration of CTLs associated with decreased functionality of this T cell compartment in the peripheral blood from patients with Chagas disease in the indeterminate phase (19). In this study we

went deeper by exploring how metabolism affects the monocyte compartment and T cell functionality during this human infectious disease. We have found that the non-classical monocyte subpopulation expanded in the peripheral blood of both asymptomatic and symptomatic chronic Chagas disease patients, being this subset an important source of NO production. Additionally, total monocytes from Chagas disease patients exhibited higher HIF-1α expression, glucose uptake and glycolytic activity relative to control donors. In agreement, glycolysis inhibition decreased IL-1β and NO production in *T. cruzi*-infected peripheral blood mononuclear cell (PBMCs) cultures and diminished T-cell nitration. Thus, the CTLs dysfunction observed in infected individuals is associated to the metabolic pathway activated in the monocyte compartment.

Results

Chagas disease patients have increased frequencies of NO+ and HIF-1α+ monocytes

Peripheral blood samples from 40 patients with Chagas disease and 55 from control donors of both sexes were collected and tested for *T. cruzi*-specific antibodies by ELISA and IHA (Table 1). The median value for anti *T. cruzi* antibody titer was 1/256 (local cutoff titer 1/32) detected by IHA. Patients were grouped according to Kuschnir classification (20): The 88% (35/40) of patients were grouped into group 0, 10% (4/40) into group 1, and 2% (1/40) into group 3.

To identify the main cellular source of NO from circulating leukocytes, we measured NO production in polymorphonuclear cells (PMNCs) and monocytes by flow cytometry following the gating strategy depicted in Figure 1A. Patients with Chagas disease exhibited higher frequency of NO-producing monocytes but no differences were detected in the percentage of NO-producing PMNCs relative to control donors (Figure 1B). Furthermore, the production of ROS by monocytes and PMNCs was similar between both groups (Supplementary Figure 1). Notably, no significant differences were found in the percentages of NO- and ROS-producing monocytes comparing patients in the asymptomatic phase (G0) versus symptomatic patients (G1-G3) ($p= 0.83$ and $p> 0.99$ respectively). Since NO production results from inducible NO synthase (iNOS) activity and this enzyme is a HIF-1α-target molecules, we evaluated HIF-1α protein expression in the monocyte population by flow cytometry. We have found that patients with Chagas disease exhibited increased frequency of HIF-1α+ monocytes in comparison with control donors, although the molecular expression levels per cell (MFI) remained unchanged (Figure 1C).

Despite the fact that hypoxia could activate an inflammatory response, HIF-1α activation leads to increase extracellular adenosine production as an essential endogenous anti-inflammatory mediator to protect tissue damage (21). Adenosine is originated from the sequential dephosphorylation of eATP, mainly by the subsequent action of CD39 and CD73

ecto-enzymes (22, 23). In line with this, we observed increased plasmatic ATP levels (Figure 1D), associated with higher frequency of circulating monocytes expressing CD39 in *T. cruzi*-infected patients compared to control donors but, we found similar expression of this ecto-enzyme per cell (MFI) in both studied groups (Figure 1E). Although we did not observe differences in the percentage of CD73+ monocytes, interestingly a higher MFI of this enzyme was detected in monocytes from seropositive patients (Figure 1F).

Monocytes from *T. cruzi*-infected patients exhibit increased functional activity

Following the gating strategy described in Figure 2A, we found that monocytes from patients showed increased frequency of IL-1β, IL-6 and IL-10production compared to control donors in response to in vitro stimulation with the pro-inflammatory stimulus (LPS). Moreover, the amount of IL-1β and IL-6 (measured as MFI), were also significantly increased in monocytes from *T. cruzi*-infected patients but no differences were observed in IL-10 levels (Figure 2B). Strikingly, under parasite lysate stimulation, intracellular production of IL-6 and IL-1β was higher in monocytes from patients than the control counterpart (Figure 2C).

The monocyte subpopulations were defined by the expression of CD14 and/or CD16 (Figure 3A). The percentage of circulating $CD14^{++}CD16^{-}$ (classical) monocytes decreased, while the frequency of $CD14^{+}CD16^{++}$ (non-classical) subset increased in seropositive patients when compared to control donors (Figure 3B) as was observed for bacterial and viral infections (24-26). The percentages of NO- and ROS--producing monocytes were significant higher in the non-classical monocyte subset than in classical monocyte subpopulation in both groups, patients and control donors (Figure 3C-D). Conversely, the proportion of non-classical monocytes producing IL-10 or IL-6 was lower than the frequency of IL-10+/IL-6+ classical monocytes (Figures 3E and F) in both studied groups. We found no differences in the frequency of non-classical monocytes from asymptomatic patients (G0)

and from those in the cardiac chronic stage (G1-G3) ($p > 0.99$). Altogether, the results clearly demonstrate that the non-classical subset of monocytes displays pro-oxidative properties.

Strikingly, Glut-1 expression exhibited a dichotomist pattern in classical and non-classical monocyte subsets between both groups. In seropositive patients non-classical monocytes exhibited increased Glut-1 expression while the main Glut-1+ subset in healthy control was classical monocytes (Figure 3G). Although CD39 expression did not show significant difference in both monocyte subpopulations (Figure 3H), increased CD73 expression was detected in non-classical monocytes in comparison with classical monocytes, in control as well as in patient samples (Figure 3I).

Monocytes from *T. cruzi*-infected patients showed increased glycolysis and mitochondrial damage

HIF-1α drives multiple immune cell effector functions, including energy metabolism. Indeed, HIF-1α–dependent glycolytic pathway orchestrates a metabolic checkpoint for the differentiation of Th17 profile (27), Tr1 cells (28) and classically-activated macrophages (29). To determine whether monocytes from patients with Chagas disease have enhanced glycolytic metabolism, we measured extracellular acidification rate (ECAR), and oxygen consumption rate (OCR), as measures of glycolysis and OXPHOS, respectively.

Higher glycolysis, glycolytic capacity and glycolytic reserve was observed in monocytes from seropositive patients compared to control donors (Figure 4A and B). Consistent with these findings, *T. cruzi*-infected patients exhibited higher frequency of Glut-1+ monocytes relative to controls (Figure 4C). Of note, monocytes from asymptomatic (G0) seropositive individuals did not exhibit differences in the glycolytic activity compared to monocytes from patients in cardiac chronic G1-G3 stages ($p > 0.99$ glycolytic activity).

Moreover, monocytes from patients showed lower respiration driving-ATP synthesis OCR and higher respiration driving proton leak in comparison with control donors (Figure 4D

and E). Consequently, monocytes from infected individuals exhibited a significant decrease of the bioenergetic health index (BHI), a proposed functional biomarker of oxidative stress in patients suffering metabolic disorders (30) (Figure 4F). To distinguish between mitochondria with altered or unaltered mitochondrial potential (31) we stained monocytes with a combination of MitoTracker Green (Δψ-independent mitochondrial stain) and MitoTracker Orange (Δψ-dependent mitochondrial stain). A significant increase in the number of dysfunctional mitochondria (MitoTracker Green^{high}, MitoTracker Orange^{low}) and in mitochondrial mass (MitoTracker Green staining) was found in monocytes from seropositive patientscompared to monocytes from control donors (Figure 4G).

Monocyte glycolysis is necessary for *T. cruzi*-induced lymphocyte nitration and dysfunction

Since glycolytic activity has been extensively associated with pro-inflammatory activities of immune cells, we characterized the effect of glycolysis on monocyte effector function during *T. cruzi* infection. To this aim in vitro infected PBMCs were pre-treated with a synthetic glucose analog 2-DG that inhibits glycolysis and compared with non-treated infected PBMCs from the same donor. We found that 2-DG treatment did not modify M1-marker (CD64) expression, but increased the M2-marker mannose receptor (CD206) expression on infected monocytes/macrophages (Mo/Ma) (Figure 5A). Moreover, glycolysis inhibition decreased the frequency of IL-6- and of IL-1β-producing Mo/Ma, as well as the amount of IL-1β released to the culture supernatant (Figure 5B and C). In contrast, glycolysis inhibition raised the percentage of IL-10-producing Mo/Ma (Figure 5D).

To evaluate the effect of monocyte glycolysis on T cell nitration, we measured NO production and TN^+ lymphocytes in infected PBMCs cultures subjected to 2-DG treatment. The glucose analog lowered the frequency of NO-producing Mo/Ma (Figure 5E), NO levels in culture supernatant (Figure 5F) as well as the frequency of T cell nitration (Figure 5G). To further define the link between monocyte glycolytic metabolism and T-cell nitration, in vitro

infected monocytes were pre-treated with 2-DG. After 3 h the monolayers were washed and co-cultured with sorted CD3+ lymphocytes. The inhibition of glycolysis decreased the percentage of TN^+ T-cells (Figure 5H). Furthermore, T-cell nitration is cell contact dependent since the disruption of physical contact between infected monocytes and T-cells abrogated the nitration of lymphocytes (Figure 5H).

To confirm that NO production by monocytes induces CTLs dysfunction during *T. cruzi* infection, we treated PBMCs from control donors with NO production-inhibitor L-NAME previous to infection. We observed that L-NAME reduced NO levels (Figure 6A), lymphocytes nitration (Figure 6B) and re-established the effector function measured by IFN-γ and TNF production by CTLs (Figure 6C) compared to untreated infected cells. Altogether, these results clearly evidence that glycolysis governs oxidative stress on monocytes and consequently regulate T cell function in the context of *T. cruzi* infection.

Our hypothesis was further confirmed by the fact that both the frequency of non-classical monocytes and the frequency of NO-producing monocytes positively correlated with the percentage of TN^+ lymphocytes in peripheral blood samples from *T. cruzi* infected patients and control donors (Figure 6D).

Discussion

Monocytes are key players in anti-parasite immune response since they produce inflammatory cytokines, inflammation-accelerating chemokines, and microbicidal species. The present study demonstrates that during human chronic *T. cruzi* infection monocytes exhibit long-lasting functional phenotypic changes, since they are more prone to produce cytokines under stimulation and they exhibited increased production of NO compared to monocytes from control donors, contrasting with the impaired effector function of the CTLs compartment (19). Cytotoxic CD8+ T cells from seropositive patients are more susceptible to apoptosis and exhibit high levels of nitrated tyrosine residues on their surface. Naïve cells constitute the main subpopulation that undergoes tyrosine nitration, and the majority of NT^- cells are effector memory CD8+ T cells. Notably, TN^+CTLs are less functional than TN^- population as TN^+CTLs exhibit deactivation of the cytotoxic function with lower expression of CD107a (a degranulation marker) and decreased production of cytokines (IFN-γ, TNF and IL-2). The nitration of surface proteins on T cells is promoted by peroxynitrites, which are induced by the reaction of NO with the superoxide anion (32-34). In the present work, we identified non-classical monocytes as an important cellular source of NO, which promotes CD8+ T cell nitration/dysfunction in this human infectious disease.

The expanded non-classical monocyte subset has been previously described in the context of different inflammation-related diseases (35-37). Regarding Chagas disease, our results are in full agreement with a recent report from Dr. Laucella´ group. They demonstrated that "*T. cruzi*-infected subjects with mild or no signs of cardiac disease showed increased levels of non-classical monocytes compared to healthy controls" (38).

In the present work, we have also found increased monocyte-expressing HIF-1α, a transcription factor that could be promoting the enhanced amount of plasmatic IL-1β observed in Chagas disease patients (19). In fact, it was recently demonstrated that activated macrophages produce IL-1β because of HIF-1α stabilization in a mechanism

supported by glycolysis (29). The metabolism of glucose into pyruvate prevents aerobic degradation of HIF-1 protein, allowing HIF-1 accumulation. Accordingly, total monocytes isolated from patients showed activated glycolytic metabolism in comparison with their control counterpart.

HIF-1 is the master regulator of metabolic adaptation to hypoxia with a broad range of effector functions. Among these, NO production is a recognized downstream effect of HIF-1α, since this transcription factor stimulates the expression of iNOS. Interestingly, although s *T.cruzi*-infected patients exhibited higher frequency of NO-producing monocytes, this mediator is not augmented in plasma from infected patients (19), which is consistent with data from the literature (39). Regarding cellular NO effector functions, Everts and coworkers demonstrated an autocrine NO effect on dendritic cell metabolism (9). They postulated the notion that NO inhibits mitochondrial electron transport by the nitrosylation of iron-sulfur-containing proteins from complex I (NADH-ubiquinone oxidoreductase), complex II (succinate-ubiquinone oxidoreductase) and complex IV (cytochrome C oxidase), thereby blocking oxygen consumption and ATP production (40-42). The direct connection between reduced respiratory rate and inflammation has been recognized for some time (43). In this sense, cells with mitochondrial damage activate the glycolytic metabolism to produce the ATP necessary to survive. Our results suggest that oxidative stress disrupts mitochondrial potential in monocytes from seropositive individuals. In turn, these cells enhance the activation of glycolytic metabolism supporting their inflammatory state.

Mitochondria are sub-cellular organelles that play vital roles into the eukaryotic cells. Even though their function in energy metabolism is extensively recognized, only few years ago several evidences have demonstrated the relevance of mitochondria in immunity (29, 44-46), and put these organelles as a platform for immune regulation (47, 48). Mitochondria function could be assessed by respiration driving ATP production, respiration driving proton leak, maximal respiration and spare respiratory capacity, among others. Each of these

parameters is sensitive to different free radicals or oxidants, clearly indicating that mitochondria are particularly susceptible to oxidative stress. In agreement with our results, a high percentage of cardiac and skeletal muscle mitochondria exhibiting structural and functional alterations was reported in Chagas disease patients even in those without clinical criteria of cardiomyopathy (49, 50). In this sense, *T. cruzi* infection provokes a significant decline in mitochondrial membrane potential (51).

Recent studies indicate mitochondrial damage products (mROS production, cytosolic release of mDNA, and the dissipation of mitochondrial membrane potential) as common factors to trigger NLRP3 inflammasome activation (52, 53). In line with these findings, we observed altered mitochondrial potential with decreased BHI in monocytes from infected individuals. Therefore, the accumulation of damaged mitochondria might give rise to the activation of NLRP3 inflammasome with the consequent induction of IL-1β production, which would account for the increased levels of this potent inflammatory cytokine observed in plasma from patients with Chagas disease. On the other hand, the release of ATP can also promote inflammasome activation. Here we have also found increased ATP plasmatic levels in *T. cruzi*-infected patients concomitant with higher monocyte expression of CD39 and CD73 ecto-enzymes, which are in charge of eATP metabolic degradation to adenosine. Thus, it is plausible that monocytes promote eATP degradation to dampen the inflammatory microenvironment. In this sense, it was described that ATP promotes HIF-1α expression (54), with the consequent ecto-nucleotidases up-regulation (55).

In vitro studies confirmed our hypothesis. Glycolysis inhibition of infected PBMCs (obtained from controls donors) suppresses *T. cruzi*-induced inflammatory Mo/Ma profile, diminishing inflammatory cytokine production and increasing IL-10^{+} cells. Of note, the increased frequency of IL-10+ Mo/Ma could be an indirect effect of glycolysis inhibition and could be the consequence of IL-1β diminution induced by 2-DG. In accordance with our previous observations, which revealed that IL-1β induces NO production (19, 56), 2-DG

reduced IL-1β production and this reduction could lead to lower cellular secretion of NO. In turn, glycolysis inhibition of infected monocytes decreased nitration of lymphocytes, an effect that depend on cell-cell contact. Supporting the in vitro results, the frequency of NO-producing monocytes positively correlated with the percentage of TN^+ lymphocytes in peripheral blood samples from control donors and patients. Through well designed experimental strategies, Koo and co-workers have recently delineated the metabolic regulation of the macrophage response to *T. cruzi*. By studying in vitro assay murine systems they found that upon infection macrophages maintain a Krebs cycle linked oxidative metabolism that allow only a partial iNOS activation. Strikingly, IFN-γ treatment "lead to complete metabolic shut down of oxidative metabolism, and enhanced the glycolytic source of energy availability in infected macrophages". This shift activates the production of optimal NO and ROS levels dampening the lack of effective microbicidal response (57).

The major achievement of the present work was to establishe that glycolysis could be a key factor that sustains the pro-oxidative monocyte profile in seropositive patients, even in those in the indeterminate (asymptomatic) chronic form of Chagas disease, also known as "silent" stage. Etiological treatment of Chagas disease is currently based on two compounds, nifurtimox and benznidazole, which have significant activity in congenital and acute *T. cruzi* infections (> 95 and 60–80% of parasitological cures, respectively). However, a major limitation of these drugs is their limited and variable curative activity in the chronic form of the disease, the most prevalent clinical presentation. Even when etiological treatment is clinically recommended, the evidence-based medicine has not been fully validated, and its use in the chronic phase of the disease is still controversial. The effect of benznidazole treatment on patients with Chagas cardiomyopathy was recently reported in a well-conducted BENEFIT trial (58). After 5 years of follow up, the results evidence that treatment with benznidazole is unlikely to have a major preventive effect on the progression of heart disease in chronic Chagas disease patients, even though the parasite load significantly

diminished. Although the exact cause-effect relation for cardiomyopathy development has not yet been revealed, the results described in the present work point out that a sustained pro-oxidative monocyte profile could be accounting for chronic state described in these patients.

In summary, altogether the results of the present study demonstrate that chronic *T. cruzi* infection sustains monocyte glycolytic metabolism and HIF-1α/NO pathway activation and expands non-classical circulating monocytes with increased oxidative potential that may induce nitration of CTLs affecting their functionality. In concert, the described mechanisms could explain the inefficient parasite clearance, concomitant with a sustained inflammatory environment that underlies the characteristic lesions of chronic Chagas disease.

Methods

Subjects and ethics statement

A total of 95 subjects were recruited at the "Hospital Nuestra Señora de la Misericordia", Córdoba and at the Instituto Nacional de Parasitología "Dr. Mario Fatala Chabén" Buenos Aires, Argentina. *T. cruzi* infection was diagnosed by indirect hemagglutination (IHA) and enzyme-linked immunosorbent assay (ELISA). Subjects positive on these two tests were considered infected. Chronic Chagas disease patients (n=40) were evaluated clinically including electrocardiogram (ECG) and chest X-rays. Subjects were grouped according to the Kuschnir grading system (20). Group 0 (G0) included seropositive individuals having a normal ECG and a normal chest X-rays; group 1 (G1) comprised seropositive patients with a normal chest X-rays but abnormalities in the ECG; group 2 (G2) encompassed seropositive patients with ECG abnormalities and heart enlargement as determined by chest X-rays and group 3 (G3) involved seropositive patients with ECG abnormalities, heart enlargement and clinical or radiological evidence of heart failure. The control group (n=55) consisted of age-matched individuals who were serologically negative for *T. cruzi*. All donors with chronic or inflammatory diseases, erythrosedimentation rate >30 mm or white blood cells count <4,000 or >10,000/mm^3 were excluded from the study.

Blood collection

Approximately 15-30 mL of peripheral blood were drawn from each individual. PBMCs were isolated through density gradient centrifugation using Ficoll-Hypaque PLUS (GE Healthcare Bioscience).

T. cruzi lysate

Protein lysate from *T. cruzi* trypomastigotes was obtained by 4 freeze/thaw cycles, which were followed by sonication. In brief, trypomastigotes from the Tulahuen strain were collected from a monolayer of infected Vero cell cultures. After washing, the parasites were

frozen and thawed 4 times. Thereafter, the sample was sonicated and the supernatant of a 12,000 g centrifugation was collected and filtered. Protein concentration was determined by Bradford technique.

Monocyte isolation and bioenergetics studies

Monocytes were purified by positive selection from PBMCs using CD14 Microbeads (EasySep, StemCell Technology), following manufacturer's instructions. Then, 300,000 cells/well were plated in triplicate of XFp cell culture microplates (Seahorse Agilent) pre-coated with polyethylenimine and centrifuged to attach monocytes. RPMI medium was replaced with 180 µL of assay medium (DMEM XF base supplemented with 2 mM glutamine, pH 7.4) for extracellular acidification rate (ECAR) measurements or with 175 µL of assay medium (DMEM XF base supplemented with 4 mM glutamine, 5.5 mM D-glucose and 1 mM pyruvate, pH 7.4) for oxygen consumption rate (OCR) determination. Plates were kept at 37°C for 45 min and loaded into Seahorse XFp extracellular flux analyzer. OCR was determined at the beginning of the assay (basal OCR) and after the sequential addition of 1 µM oligomycin, 1 µM FCCP and 0.5 µM rotenone plus antimycin A. Monocytes were titrated with 0.125-2 µM FCCP and 1 µM FCCP rendered the maximum OCR, so this concentration was used for the experiments. Non-mitochondrial OCR was determined after the addition of 0.5 µM rotenone plus antimycin A and subtracted from all other values before calculating the respiratory parameters, as previously described (59). Respiratory parameters were obtained as follows: basal respiration, baseline OCR; respiration driving proton leak, OCR after oligomycin addition; respiration driving ATP synthesis, basal respiration–respiration driving proton leak; maximum respiration, OCR after FCCP addition; spare respiratory capacity, maximum respiration–basal respiration. Values were expressed as a percentage of OCR corresponding to the last baseline rate (100%). ECAR was determined at the beginning of the assay and after the sequential addition of 10 mM d-glucose, 1 µM oligomycin and 100 mM 2-deoxy-D-glucose (2-DG). Glycolytic parameters were obtained as follows: glycolysis,

ECAR after glucose addition–basal ECAR; glycolytic capacity, ECAR after oligomycin addition–basal ECAR; glycolytic reserve, glycolytic capacity–glycolysis. Values were expressed as a percentage of ECAR corresponding to the last basal rate (100%). Non-glycolytic ECAR was determined after the addition of 100 mM 2-DG and subtracted from all other values before calculating the glycolytic parameters.

The bioenergetic health index (BHI) was estimated according to the equation from Chacko et al. (60)

$$BHI = \frac{\text{Spare respiratory capacity } \times \text{ ATP production}}{\text{Non} - \text{mithocondrial respiration } \times \text{ Proton leak}}$$

Ex Vivo flow cytometry

Peripheral blood was lysed with ACK lysing buffer to remove erythrocytes, cells were blocked with Fc block and stained with anti-CD14-PECy5 (eBioscience; Cat:15-0149-41, Clone:61D3), anti-CD16-PECy7 (eBioscience; Cat: 25-0168-41, Clone:CB16), anti-CD39-biotin (Biolegend; Cat: 328204, Clone:1A) and Streptavidin-APC (eBioscience; Cat: 17-4317), anti-CD73-PE (Biolegend; Cat: 344003, Clone:A2D), anti-Glut-1-PE (R&D Systems; Cat: FAB1418P, Clone: 202915), anti-NT rabbit (Sigma-Aldrich; Cat: N 0409) and anti-rabbit-Alexa 647 (ThermoFisher, Cat: A-21244). To determine HIF-1α expression, cells were permeabilized with FOXP3 staining buffer set (eBioscience) and labeled with anti-HIF-1α rabbit (Abcam; Cat: AB51608, Clone: EP1215Y) followed either by anti-rabbit-Alexa 488 (ThermoFisher, Cat: A11034) or anti-rabbit-Alexa 647 (ThermoFisher, Cat: A21244) antibodies. Data was acquired with a FACS Canto II flow cytometer (Becton Dickinson) and analyzed using the FlowJo sofware.

ATP quantification

ATP levels were quantified in plasma from individuals by ATP Determination Kit (Invitrogen™), according to the manufacturer's instructions. Briefly, samples were incubated

with luminescent reaction mix at room temperature for 30 min in a 96-well white plate protected from light. Luminescence was measured at 560 nm in a Synergy 2 Multi-Mode Reader (BioTek). A standard curve was plotted to calculate the ATP concentration and a regression analysis was applied. It is important to stress that plasma samples were separated from formed elements 35 min after blood collection.

Measurement of mitochondrial contents

PBMCs were stained with anti-CD14-PECy5 (eBioscience; Cat:15-0149-41, Clone:61D3), anti-CD16-PECy7 (eBioscience; Cat: 25-0168-41, Clone: CB16) and then MitoTracker Green and MitoSpy Orange stainings were performed, according to manufacturer's instructions (Biolegend) and analyzed by flow cytometry.

Intracellular cytokine measurement

PBMCs were cultured with monensin (Golgistop; 0.6 µl/ml; BD Biosciences), brefeldin A (Golgiplug; 1µl/ml; BD Biosciences) and parasite lysate (10µg/mL) for 16h or LPS (100 ng/mL; Sigma) for 4 h (61), and stained with anti-CD14-PECy5 (eBioscience; Cat:15-0149-41, Clone:61D3), anti-CD16-PECy7 (eBioscience; Cat: 25-0168-41, Clone: CB16). After staining of surface markers, cells were fixed and made permeable according to the manufacturer's instructions BD Cytofix/Cytoperm™ Kit (BD Biosciences). Then the cells were stained with anti-IL-1β-FITC (eBioscience; Cat: BMS127, Clone:B-A15), anti-IL-6-PE (Immunotools; Cat: 21670064, Clone: 8C9), and anti-IL-10-APC (Biolegend; Cat: 501419, Clone: JES3-9D7) antibodies, and analyzed by flow cytometry.

Measurement of reactive oxygen (ROS) and nitrogen species

ROS and NO production were evaluated using the molecular probes: H2DCF-DA and DAF-FM DA (10 µM), respectively and analyzed by flow cytometry. After surface staining, the cells were re-suspended in 100 µL of RPMI and 100 µL of 2′,7′ dichlorodihydrofluorescein diacetate 20 µM (H2DCFDA) or 100 µL of DAF-FM DA 20 µM

(Molecular Probes, Eugene, OR, USA) were loaded onto cells in clear bottom, black walled plates (Fisher Scientific). Cells were incubated for 30 min at 37ºC, washed twice with PBS, and then loaded with 300 µL of PBS. Fluorescence of oxidized product was measured at excitation/emission of 488/520 nm using the FACs Canto II (BD Bioscience). The nitrite/nitrate content, indicative of NO production, was monitored by the Griess reagent assay (62).

Culture of PBMCs and glycolysis inhibition

Vero cell monolayers were infected with *T. cruzi* Tulahuen trypomastigotes for 3 h, washed and maintained in RPMI at 37°C in a 5% CO2 atmosphere. After 7 days, the parasites were collected from the supernatant of infected cells and harvested by centrifugation and washed. PBMCs from 8 control donors were seeded at 2.5 x 10^5 cells/well and treated with 2-DG (11mM, R&D Systems) or maintained in medium for 1 h, and then washed and cultured with *T. cruzi* Tulahuen trypomastigotes (1:1 rate) for 3 h; then, the cells were washed. After 24 h, culture supernatants were evaluated for NO levels, and the cells stained with anti-CD14-PECy5 (eBioscience; Cat:15-0149-41, Clone:61D3), anti-CD64-APCCy7 (Biolegend; Cat: 305026, Clone: 10.1), anti-CD206-Alexa 647 (Biolegend; Cat: 321116, Clone: 42050), anti-IL-1β-FITC (eBioscience; Cat: BMS127, Clone:B-A15), anti-IL-6-PE (Immunotools; Cat: 21670064, Clone: 8C9), anti-IL-10-PECy7 (Biolegend; Cat: 501419, Clone: JES3-9D7) antibodies, anti-Nitrotyrosine antibody produced in rabbit (Sigma-Aldrich; Cat: N 0409) and anti-rabbit-Alexa 647 antibody (ThermoFisher, Cat: A-21244), and NO production (Molecular Probes; Cat: D23842) by flow cytometry.

Transwell co-culture assay

PBMCs obtained from buffy coats from healthy donors were diluted 1:2 times with supplemented RPMI and layered on Ficoll Hypaque (Sigma Aldrich). Lymphocytes and monocytes were further purified from PBMCs by sorting. To obtain highly purified T lymphocytes and monocytes, PMBCs were labeled with anti-CD3 Alexa Fluor 488 (BD

Biosciences Cat: 557694, Clone: UCTH1) and anti-CD14 PECy5 (eBioscience; Cat:15-0149-41, Clone:61D3) for 20 min at 4°C and sorted using FACS Aria II (Beckton Dickinson). Monocytes were seeded in the lower chamber of 24-well plate at a concentration of 500.000 cells/well and were treated with 2-DG (11 mM; R&D Systems) or maintained in medium for 1 h. The monolayers were washed and monocytes were infected with *T. cruzi* trypomastigotes (1:1 rate) for 3 h, and then washed. CD3+ cells (3.5 x 10^5 cells/well) were plated on top of the transwell inserts or directly co-cultured with infected monocytes and incubated overnight at 37°C, 5% CO_2 incubator. The cells were then harvested and stained with anti-CD14 PECy5 (eBioscience; Cat:15-0149-41, Clone:61D3), anti-CD3 Alexa Fluor 488 (BD; Cat: 557694, Clone: UCTH1), anti-CD8 APCCy7 (BD; Cat: 557834, Clone: SK1), anti-Glut-1 PE (R&D Systems; Cat: FAB1418P, Clone: 202915), rabbit anti-Nitrotyrosine (Sigma Aldrich; Cat: N0409) and anti-rabbit Alexa 647 (ThermoFisher, Cat: A-21244) antibodies, for flow cytometry.

Statistical analysis

Statistical analysis was performed with GraphPad Prism 5.0 software. Student *t-test* or Mann-Whitney test were used according to data distribution for statistical analysis when independent two groups were analyzed. For paired samples, parametric paired *t-test* or non-parametric Wilcoxon test were used, according to data distribution. For comparison between more than 2 groups the data obtained were analyzed by ANOVA with post-hoc Tukey test. Pearson correlation coefficient was used to evaluate the association between two parametric variables. Statistical significance was set at $*p\text{-values} < 0.05$.

Study approval

This study was reviewed and approved by the Comité Institucional de Ética de la Investigación en Salud del Adulto, Ministerio de Salud de la Provincia de Córdoba (Act # 194/2014) and by the Comité de Ética del Instituto Nacional de Parasitología “Dr. Mario Fatala Chaben”, Buenos Aires, Argentina. All studies were conducted according to the

principles expressed in the Declaration of Helsinki. Signed informed consent was obtained from each donor included in the study.

Author contribution

Conceived and designed the experiments: LMS and MPA. Performed the experiments: LMS, NE, GB, LPQP, PMA, LMV, EACS and MPA. Analyzed the data: LMS, NE, GB, LPQP, PMA, LMV, ARM, EACS, YHV, LM, MP and MPA. Patients handling and human samples: LPQP, LMV, ARM, YHV and MP. Wrote the paper: LMS and MPA.

Acknowledgments

The authors would like to thank Dr. Francisco Quintana (Harvard Institute of Medicine) for the careful revision of the manuscript. The authors also thank Laura Gatica, Gabriela Furlán, Alejandra Romero, Pilar Crespo, and Paula Abadie for their skillful technical assistance. They also thank Susana Guignard, Yamile Ana, Nicolás Eric Ponce, Maria Cecilia Ramello, Andrea Errasti, the staff of Biochemical Laboratory of Diagnosis from the Hospital Nuestra Señora de la Misericordia and from Instituto Nacional de Parasitología “Dr. Mario Fatala Chaben” and Claudia Carabajal (Director of Blood Bank from Universidad Nacional de Córdoba) for their collaboration. EACS, LM, MP and MPA are members of the scientific career from the Consejo Nacional de Investigaciones Científicas y Técnicas de la República Argentina (CONICET). GB, LS, NE, and PMA thank CONICET for the fellowships granted; LV and LPQP thank fellowship granted from Fundación Florencio Fiorini and ANPCyT-FONCyT, respectively. GB thanks Consejo Interuniversitario Nacional (CIN) for the fellowship granted. This work was funded by Secretaría de Ciencia y Tecnología, Universidad Nacional de Córdoba (SECyT-UNC), Fondo para la Investigación Científica y Tecnológica from Agencia Nacional de Promoción Científica y Tecnológica (ANPCyT-FONCyT) (PICT 2013-2885 and PICT 2015-1130) and by Consejo Nacional de Investigaciones Científicas y Técnicas (CONICET) (PIP 11220120100620).

References:

1. Ziegler-Heitbrock L, Ancuta P, Crowe S, Dalod M, Grau V, Hart DN, Leenen PJ, Liu YJ, MacPherson G, Randolph GJ, et al. Nomenclature of monocytes and dendritic cells in blood. *Blood.* 2010;116(16):e74-80.
2. Ziegler-Heitbrock L. Blood Monocytes and Their Subsets: Established Features and Open Questions. *Frontiers in immunology.* 2015;6(423.
3. Sanmarco LM, Eberhardt N, Ponce NE, Cano RC, Bonacci G, and Aoki MP. New Insights into the Immunobiology of Mononuclear Phagocytic Cells and Their Relevance to the Pathogenesis of Cardiovascular Diseases. *Frontiers in immunology.* 2018;8(1921.
4. Hayashi M, Sakata M, Takeda T, Yamamoto T, Okamoto Y, Sawada K, Kimura A, Minekawa R, Tahara M, Tasaka K, et al. Induction of glucose transporter 1 expression through hypoxia-inducible factor 1alpha under hypoxic conditions in trophoblast-derived cells. *The Journal of endocrinology.* 2004;183(1):145-54.
5. Calvert JW, Cahill J, Yamaguchi-Okada M, and Zhang JH. Oxygen treatment after experimental hypoxia-ischemia in neonatal rats alters the expression of HIF-1alpha and its downstream target genes. *Journal of applied physiology.* 2006;101(3):853-65.
6. Liu Y, Li YM, Tian RF, Liu WP, Fei Z, Long QF, Wang XA, and Zhang X. The expression and significance of HIF-1alpha and GLUT-3 in glioma. *Brain research.* 2009;1304(149-54.
7. Gabriely G, Wheeler MA, Takenaka MC, and Quintana FJ. Role of AHR and HIF-1alpha in Glioblastoma Metabolism. *Trends Endocrinol Metab.* 2017;28(6):428-36.
8. Colegio OR, Chu NQ, Szabo AL, Chu T, Rhebergen AM, Jairam V, Cyrus N, Brokowski CE, Eisenbarth SC, Phillips GM, et al. Functional polarization of tumour-associated macrophages by tumour-derived lactic acid. *Nature.* 2014;513(7519):559-63.
9. Everts B, Amiel E, van der Windt GJ, Freitas TC, Chott R, Yarasheski KE, Pearce EL, and Pearce EJ. Commitment to glycolysis sustains survival of NO-producing inflammatory dendritic cells. *Blood.* 2012;120(7):1422-31.
10. Metzen E, Zhou J, Jelkmann W, Fandrey J, and Brune B. Nitric oxide impairs normoxic degradation of HIF-1alpha by inhibition of prolyl hydroxylases. *Molecular biology of the cell.* 2003;14(8):3470-81.
11. Baez AL, Lo Presti MS, Fretes R, Diaz C, Pons P, Bazan PC, Strauss M, Rivarola HW, and Paglini-Oliva P. Chronic indeterminate phase of Chagas' disease: mitochondrial involvement in infection with two strains. *Parasitology.* 2013;140(3):414-21.
12. Ribeiro AL, and Rocha MO. [Indeterminate form of Chagas disease: considerations about diagnosis and prognosis]. *Revista da Sociedade Brasileira de Medicina Tropical.* 1998;31(3):301-14.
13. Gutierrez FR, Guedes PM, Gazzinelli RT, and Silva JS. The role of parasite persistence in pathogenesis of Chagas heart disease. *Parasite Immunol.* 2009;31(11):673-85.
14. Machado FS, Jelicks LA, Kirchhoff LV, Shirani J, Nagajyothi F, Mukherjee S, Nelson R, Coyle CM, Spray DC, de Carvalho AC, et al. Chagas heart disease: report on recent developments. *Cardiology in review.* 2012;20(2):53-65.
15. Machado FS, Tyler KM, Brant F, Esper L, Teixeira MM, and Tanowitz HB. Pathogenesis of Chagas disease: time to move on. *Front Biosci (Elite Ed).* 2012;4(1743-58.
16. Marin-Neto JA, Cunha-Neto E, Maciel BC, and Simoes MV. Pathogenesis of chronic Chagas heart disease. *Circulation.* 2007;115(9):1109-23.
17. Tarleton R. Parasite persistence in the aetiology of Chagas disease. *Int J Parasitol.* 2001;31(5-6):550-4.
18. Tarleton RL. Parasite persistence in the aetiology of Chagas disease. *Int J Parasitol.* 2001;31(5-6):550-4.
19. Sanmarco LM, Visconti LM, Eberhardt N, Ramello MC, Ponce NE, Spitale NB, Vozza ML, Bernardi GA, Gea S, Minguez AR, et al. IL-6 Improves the Nitric Oxide-Induced Cytotoxic CD8+ T Cell Dysfunction in Human Chagas Disease. *Front Immunol.* 2016;7(626.
20. Kuschnir E, Sgammini H, Castro R, Evequoz C, Ledesma R, and Brunetto J. [Evaluation of cardiac function by radioisotopic angiography, in patients with chronic Chagas cardiopathy]. *Arquivos brasileiros de cardiologia.* 1985;45(4):249-56.

587 21. Bowser JL, Phan LH, and Eltzschig HK. The Hypoxia-Adenosine Link during Intestinal Inflammation. *J*
588 *Immunol.* 2018;200(3):897-907.
589 22. Zimmermann H. 5'-Nucleotidase: molecular structure and functional aspects. *The Biochemical journal.*
590 1992;285 (Pt 2)(345-65.
591 23. Zimmermann H. Extracellular metabolism of ATP and other nucleotides. *Naunyn-Schmiedeberg's*
592 *archives of pharmacology.* 2000;362(4-5):299-309.
593 24. Skrzeczynska J, Kobylarz K, Hartwich Z, Zembala M, and Pryjma J. CD14+CD16+ monocytes in the
594 course of sepsis in neonates and small children: monitoring and functional studies. *Scand J Immunol.*
595 2002;55(6):629-38.
596 25. Zhang JY, Zou ZS, Huang A, Zhang Z, Fu JL, Xu XS, Chen LM, Li BS, and Wang FS. Hyper-activated pro-
597 inflammatory CD16 monocytes correlate with the severity of liver injury and fibrosis in patients with
598 chronic hepatitis B. *PloS one.* 2011;6(3):e17484.
599 26. Han J, Wang B, Han N, Zhao Y, Song C, Feng X, Mao Y, Zhang F, Zhao H, and Zeng H.
600 CD14(high)CD16(+) rather than CD14(low)CD16(+) monocytes correlate with disease progression in
601 chronic HIV-infected patients. *Journal of acquired immune deficiency syndromes.* 2009;52(5):553-9.
602 27. Shi LZ, Wang R, Huang G, Vogel P, Neale G, Green DR, and Chi H. HIF1alpha-dependent glycolytic
603 pathway orchestrates a metabolic checkpoint for the differentiation of TH17 and Treg cells. *J Exp*
604 *Med.* 2011;208(7):1367-76.
605 28. Mascanfroni ID, Takenaka MC, Yeste A, Patel B, Wu Y, Kenison JE, Siddiqui S, Basso AS, Otterbein LE,
606 Pardoll DM, et al. Metabolic control of type 1 regulatory T cell differentiation by AHR and HIF1-alpha.
607 *Nature medicine.* 2015;21(6):638-46.
608 29. Tannahill GM, Curtis AM, Adamik J, Palsson-McDermott EM, McGettrick AF, Goel G, Frezza C, Bernard
609 NJ, Kelly B, Foley NH, et al. Succinate is an inflammatory signal that induces IL-1beta through HIF-
610 1alpha. *Nature.* 2013;496(7444):238-42.
611 30. Chacko BK, Zhi D, Darley-Usmar VM, and Mitchell T. The Bioenergetic Health Index is a sensitive
612 measure of oxidative stress in human monocytes. *Redox Biol.* 2016;8(43-50.
613 31. Tal MC, Sasai M, Lee HK, Yordy B, Shadel GS, and Iwasaki A. Absence of autophagy results in reactive
614 oxygen species-dependent amplification of RLR signaling. *Proceedings of the National Academy of*
615 *Sciences of the United States of America.* 2009;106(8):2770-5.
616 32. Lu T, and Gabrilovich DI. Molecular pathways: tumor-infiltrating myeloid cells and reactive oxygen
617 species in regulation of tumor microenvironment. *Clin Cancer Res.* 2012;18(18):4877-82.
618 33. Nagaraj S, and Gabrilovich DI. Tumor escape mechanism governed by myeloid-derived suppressor
619 cells. *Cancer research.* 2008;68(8):2561-3.
620 34. Nagaraj S, Schrum AG, Cho HI, Celis E, and Gabrilovich DI. Mechanism of T cell tolerance induced by
621 myeloid-derived suppressor cells. *J Immunol.* 2010;184(6):3106-16.
622 35. Antonelli LR, Leoratti FM, Costa PA, Rocha BC, Diniz SQ, Tada MS, Pereira DB, Teixeira-Carvalho A,
623 Golenbock DT, Goncalves R, et al. The CD14+CD16+ inflammatory monocyte subset displays increased
624 mitochondrial activity and effector function during acute Plasmodium vivax malaria. *PLoS*
625 *Pathog.*10(9):e1004393.
626 36. Mukherjee R, Kanti Barman P, Kumar Thatoi P, Tripathy R, Kumar Das B, and Ravindran B. Non-
627 Classical monocytes display inflammatory features: Validation in Sepsis and Systemic Lupus
628 Erythematous. *Scientific reports.* 2015;5(13886.
629 37. Palmer CS, Anzinger JJ, Zhou J, Gouillou M, Landay A, Jaworowski A, McCune JM, and Crowe SM.
630 Glucose transporter 1-expressing proinflammatory monocytes are elevated in combination
631 antiretroviral therapy-treated and untreated HIV+ subjects. *J Immunol.* 2014;193(11):5595-603.
632 38. Perez-Mazliah DE, Castro Eiro MD, Alvarez MG, Lococo B, Bertocchi G, Cesar G, Natale MA, Albareda
633 MC, Viotti R, and Laucella SA. Distinct monocyte subset phenotypes in patients with different clinical
634 forms of chronic Chagas disease and seronegative dilated cardiomyopathy. *PLoS Negl Trop Dis.*
635 2018;12(10):e0006887.
636 39. Dhiman M, Estrada-Franco JG, Pando JM, Ramirez-Aguilar FJ, Spratt H, Vazquez-Corzo S, Perez-Molina
637 G, Gallegos-Sandoval R, Moreno R, and Garg NJ. Increased myeloperoxidase activity and protein
638 nitration are indicators of inflammation in patients with Chagas' disease. *Clinical and vaccine*
639 *immunology : CVI.* 2009;16(5):660-6.

640 40. Beltran B, Mathur A, Duchen MR, Erusalimsky JD, and Moncada S. The effect of nitric oxide on cell
641 respiration: A key to understanding its role in cell survival or death. *Proceedings of the National*
642 *Academy of Sciences of the United States of America.* 2000;97(26):14602-7.
643 41. Cleeter MW, Cooper JM, Darley-Usmar VM, Moncada S, and Schapira AH. Reversible inhibition of
644 cytochrome c oxidase, the terminal enzyme of the mitochondrial respiratory chain, by nitric oxide.
645 Implications for neurodegenerative diseases. *FEBS letters.* 1994;345(1):50-4.
646 42. Clementi E, Brown GC, Feelisch M, and Moncada S. Persistent inhibition of cell respiration by nitric
647 oxide: crucial role of S-nitrosylation of mitochondrial complex I and protective action of glutathione.
648 *Proceedings of the National Academy of Sciences of the United States of America.* 1998;95(13):7631-
649 6.
650 43. Ip WKE, Hoshi N, Shouval DS, Snapper S, and Medzhitov R. Anti-inflammatory effect of IL-10 mediated
651 by metabolic reprogramming of macrophages. *Science.* 2017;356(6337):513-9.
652 44. Nemeth B, Doczi J, Csete D, Kacso G, Ravasz D, Adams D, Kiss G, Nagy AM, Horvath G, Tretter L, et al.
653 Abolition of mitochondrial substrate-level phosphorylation by itaconic acid produced by LPS-induced
654 Irg1 expression in cells of murine macrophage lineage. *FASEB journal : official publication of the*
655 *Federation of American Societies for Experimental Biology.* 2016;30(1):286-300.
656 45. Palsson-McDermott EM, Curtis AM, Goel G, Lauterbach MA, Sheedy FJ, Gleeson LE, van den Bosch
657 MW, Quinn SR, Domingo-Fernandez R, Johnston DG, et al. Pyruvate kinase M2 regulates Hif-1alpha
658 activity and IL-1beta induction and is a critical determinant of the warburg effect in LPS-activated
659 macrophages. *Cell metabolism.* 2015;21(1):65-80.
660 46. Van den Bossche J, Baardman J, Otto NA, van der Velden S, Neele AE, van den Berg SM, Luque-Martin
661 R, Chen HJ, Boshuizen MC, Ahmed M, et al. Mitochondrial Dysfunction Prevents Repolarization of
662 Inflammatory Macrophages. *Cell reports.* 2016;17(3):684-96.
663 47. Mills EL, Kelly B, and O'Neill LAJ. Mitochondria are the powerhouses of immunity. *Nature*
664 *immunology.* 2017;18(5):488-98.
665 48. Weinberg SE, Singer BD, Steinert EM, Martinez CA, Mehta MM, Martinez-Reyes I, Gao P, Helmin KA,
666 Abdala-Valencia H, Sena LA, et al. Mitochondrial complex III is essential for suppressive function of
667 regulatory T cells. *Nature.* 2019.
668 49. Guzman Mentesana G, Baez AL, Lo Presti MS, Dominguez R, Cordoba R, Bazan C, Strauss M, Fretes R,
669 Rivarola HW, and Paglini-Oliva P. Functional and structural alterations of cardiac and skeletal muscle
670 mitochondria in heart failure patients. *Archives of medical research.* 2014;45(3):237-46.
671 50. Vyatkina G, Bhatia V, Gerstner A, Papaconstantinou J, and Garg N. Impaired mitochondrial respiratory
672 chain and bioenergetics during chagasic cardiomyopathy development. *Biochimica et biophysica acta.*
673 2004;1689(2):162-73.
674 51. Gupta S, Bhatia V, Wen JJ, Wu Y, Huang MH, and Garg NJ. Trypanosoma cruzi infection disturbs
675 mitochondrial membrane potential and ROS production rate in cardiomyocytes. *Free radical biology*
676 *& medicine.* 2009;47(10):1414-21.
677 52. Zhou R, Yazdi AS, Menu P, and Tschopp J. A role for mitochondria in NLRP3 inflammasome activation.
678 *Nature.* 2011;469(7329):221-5.
679 53. Gurung P, Lukens JR, and Kanneganti TD. Mitochondria: diversity in the regulation of the NLRP3
680 inflammasome. *Trends in molecular medicine.* 2015;21(3):193-201.
681 54. Amoroso F, Falzoni S, Adinolfi E, Ferrari D, and Di Virgilio F. The P2X7 receptor is a key modulator of
682 aerobic glycolysis. *Cell death & disease.* 2012;3(e370.
683 55. Eltzschig HK, Ibla JC, Furuta GT, Leonard MO, Jacobson KA, Enjyoji K, Robson SC, and Colgan SP.
684 Coordinated adenine nucleotide phosphohydrolysis and nucleoside signaling in posthypoxic
685 endothelium: role of ectonucleotidases and adenosine A2B receptors. *J Exp Med.* 2003;198(5):783-96.
686 56. Sanmarco LM, Ponce NE, Visconti LM, Eberhardt N, Theumer MG, Minguez AR, and Aoki MP. IL-6
687 promotes M2 macrophage polarization by modulating purinergic signaling and regulates the lethal
688 release of nitric oxide during Trypanosoma cruzi infection. *Biochimica et biophysica acta.*
689 2017;1863(4):857-69.
690 57. Koo SJ, Szczesny B, Wan X, Putluri N, and Garg NJ. Pentose Phosphate Shunt Modulates Reactive
691 Oxygen Species and Nitric Oxide Production Controlling Trypanosoma cruzi in Macrophages. *Frontiers*
692 *in immunology.* 2018;9(202.

693 58. Morillo CA, Marin-Neto JA, Avezum A, Sosa-Estani S, Rassi A, Jr., Rosas F, Villena E, Quiroz R, Bonilla R,
694 Britto C, et al. Randomized Trial of Benznidazole for Chronic Chagas' Cardiomyopathy. *N Engl J Med.*
695 2015;373(14):1295-306.
696 59. Choi SW, Gerencser AA, Ng R, Flynn JM, Melov S, Danielson SR, Gibson BW, Nicholls DG, Bredesen DE,
697 and Brand MD. No consistent bioenergetic defects in presynaptic nerve terminals isolated from
698 mouse models of Alzheimer's disease. *The Journal of neuroscience : the official journal of the Society*
699 *for Neuroscience.* 2012;32(47):16775-84.
700 60. Chacko BK, Kramer PA, Ravi S, Benavides GA, Mitchell T, Dranka BP, Ferrick D, Singal AK, Ballinger SW,
701 Bailey SM, et al. The Bioenergetic Health Index: a new concept in mitochondrial translational
702 research. *Clinical science.* 2014;127(6):367-73.
703 61. Schultz C. Intracytoplasmic detection of proinflammatory cytokines and chemokines in monocytes by
704 flow cytometry. *Methods Mol Biol.* 2003;215(29-39.
705 62. Tsikas D. Analysis of nitrite and nitrate in biological fluids by assays based on the Griess reaction:
706 appraisal of the Griess reaction in the L-arginine/nitric oxide area of research. *Journal of*
707 *chromatography B, Analytical technologies in the biomedical and life sciences.* 2007;851(1-2):51-70.

708

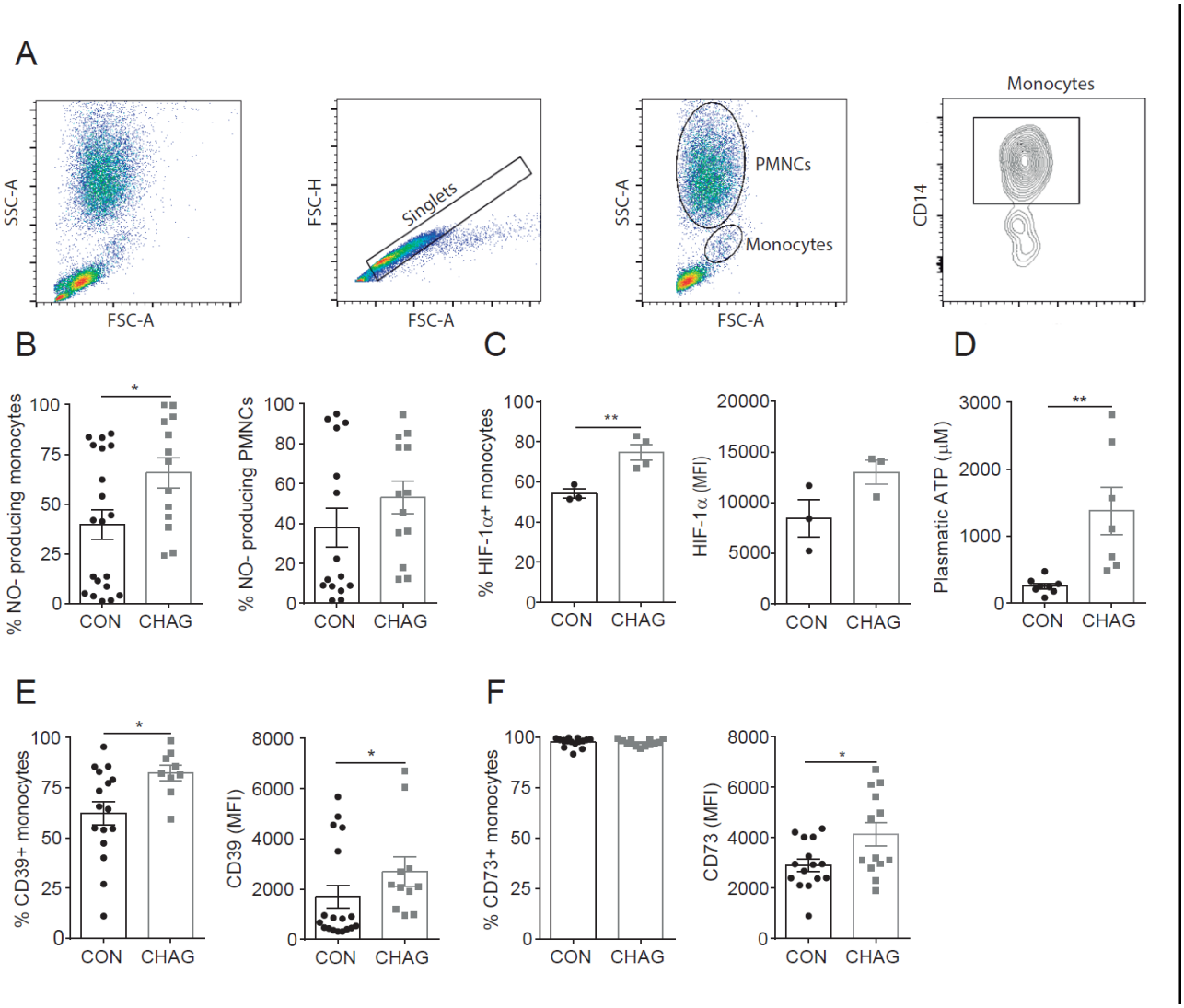

Figure 1: Patients with Chagas disease show increased frequency of NO+ and HIF-1α+ monocytes

(A) Flow cytometry gating strategy for leukocytes from peripheral blood samples. After exclusion of doublets and debris by using forward light scatter-height (FSC-H) vs. forward light scatter-area (FSC-A) density dot plots, polymorphonuclear cells (PMNCs) and monocytes were gated according to their FSC-A vs. SSC-A features. Monocytes were further identified by CD14-positive staining. **(B)** Frequency of NO-producing circulating monocytes and PMNCs from control donors (CON; n=20) and Chagas patients (CHAG; n=13). **(C)** Frequency and FMI of HIF-1α+ monocytes from CHAG (n=4) and CON (n=4). **(D)** ATP levels in plasma from CON (n=8) and CHAG (n=8). Frequency and MFI of **(E)** CD39+ and **(F)** CD73+ monocytes from CON (n=16) and CHAG (n=13). Data are presented as mean ± SEM.* $p < 0.05$, ** $p < 0.01$ (Student´s t test or Mann-Whitney test).

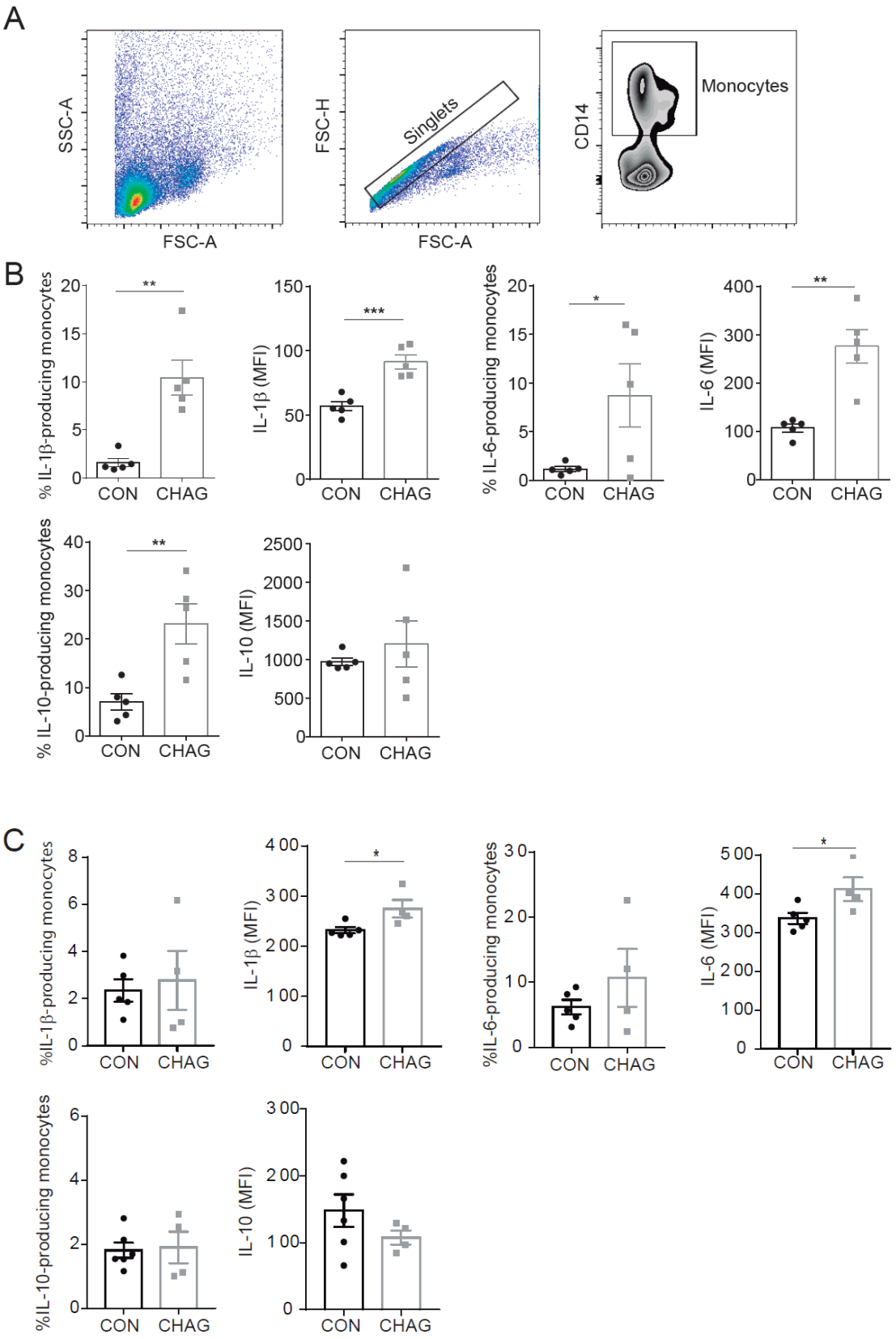

Figure 2: Monocytes from *T. cruzi*-infected patients exhibit higher functional activity potential **(A)** For intracellular cytokine analysis PBMCs isolated from peripheral blood from control donors and from seropositive patients were cultured with monensin, brefeldin A and **(B)** LPS (CON, n=5; CHAG, n=5) or **(C)** parasite lysate (CON, n=6; CHAG, n=4) and stained with

anti-CD14-PECy5. After staining of surface markers, cells were fixed and made permeable. Then the cells were stained with anti-IL-1β, anti-IL-6, and anti-IL-10 antibodies, and analyzed by flow cytometry. PBMCs were gated according to their CD14-positive staining after exclusion of doublets and debris by using FSC-H/FSC-A dot plots. Frequency and mean fluorescence intensity (MFI) of IL-1β, IL-6 and IL-10-producing monocytes. Data are presented as mean ± SEM. * $p < 0.05$, ** $p < 0.01$, *** $p < 0.001$(Student´s t test or Mann-Whitney test).

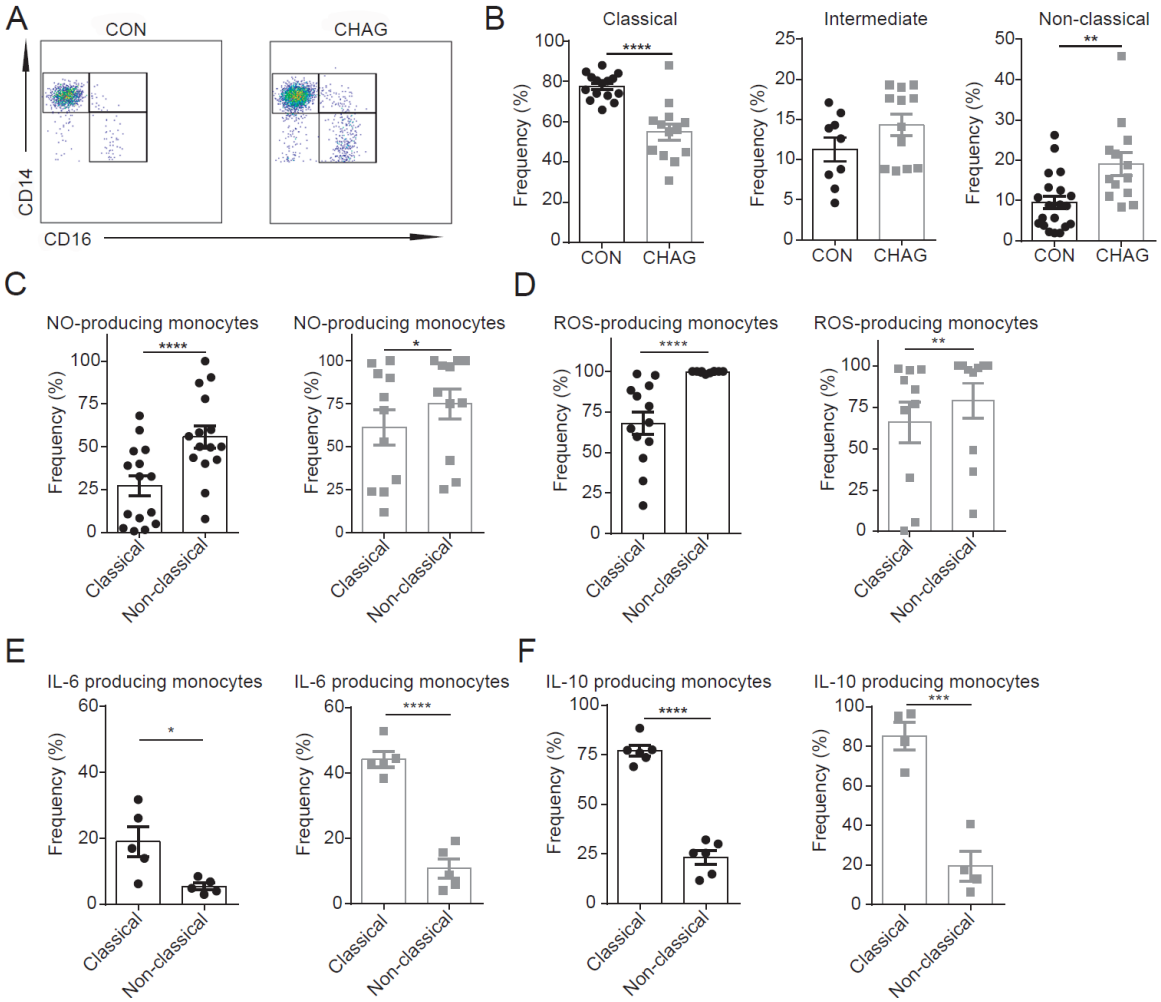
A
CON
CHAG
CD14
CD16
B
Classical
Intermediate
Non-classical
Frequency (%)
CON
CHAG
C
NO-producing monocytes
D
ROS-producing monocytes
Classical
Non-classical
E
IL-6 producing monocytes
F
IL-10 producing monocytes

739

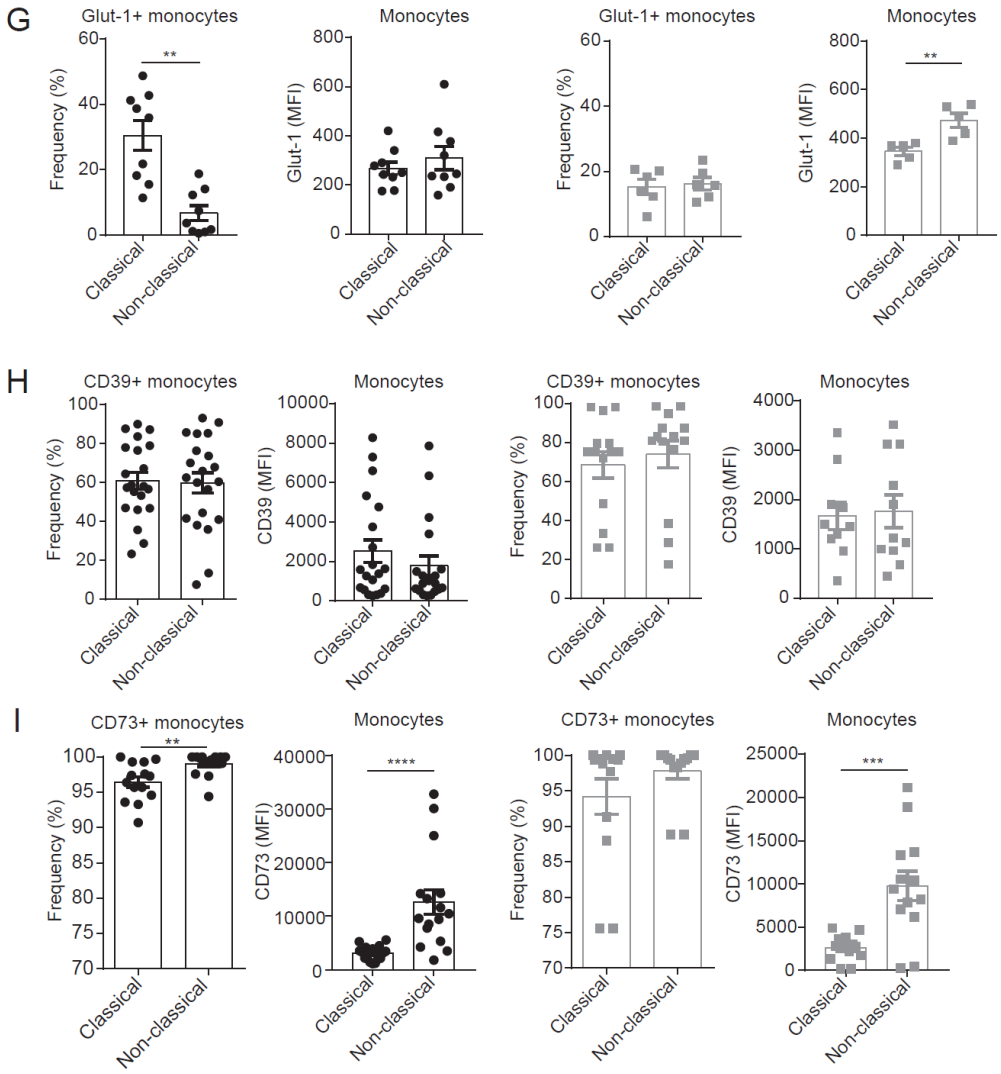

Figure 3: <u>Chagas disease patients exhibit increased frequency of non-classical monocytes</u>
(A) Representative dot plots of CD14 vs CD16 monocyte subsets in peripheral blood from control donors (CON) and from seropositive patients (CHAG). **(B)** Frequency of classical (CD14++CD16-), intermediate (CD14++CD16+) and non-classical (CD14+CD16++) monocytes from CON (n=20) and CHAG (n=13). **(C)** Percentage and mean fluorescence intensity (MFI) of NO+ (CON, n=15; CHAG, n=11), **(D)** ROS+ (CON, n=13; CHAG, n=10), **(E)** IL-6+ (CON, n=5; CHAG, n=5), **(F)** IL-10+ (CON, n=5; CHAG, n=5), **(G)** Glut-1+ (CON, n=12; CHAG, n=6), **(H)** CD39+ (CON, n=21; CHAG, n=14), and **(I)** CD73+ cells (CON, n=15; CHAG, n=15) gated in classical vs. non-classical monocytes from CON (black plots) and CHAG (grey plots). For intracellular cytokine analysis, the cells were processed as in Figure 2 and stimulated with LPS. Data are presented as mean ± SEM. * $p < 0.05$, ** $p < 0.01$, *** $p < 0.001$ and **** $p < 0.0001$ (Student´s t test or Mann-Whitney test).

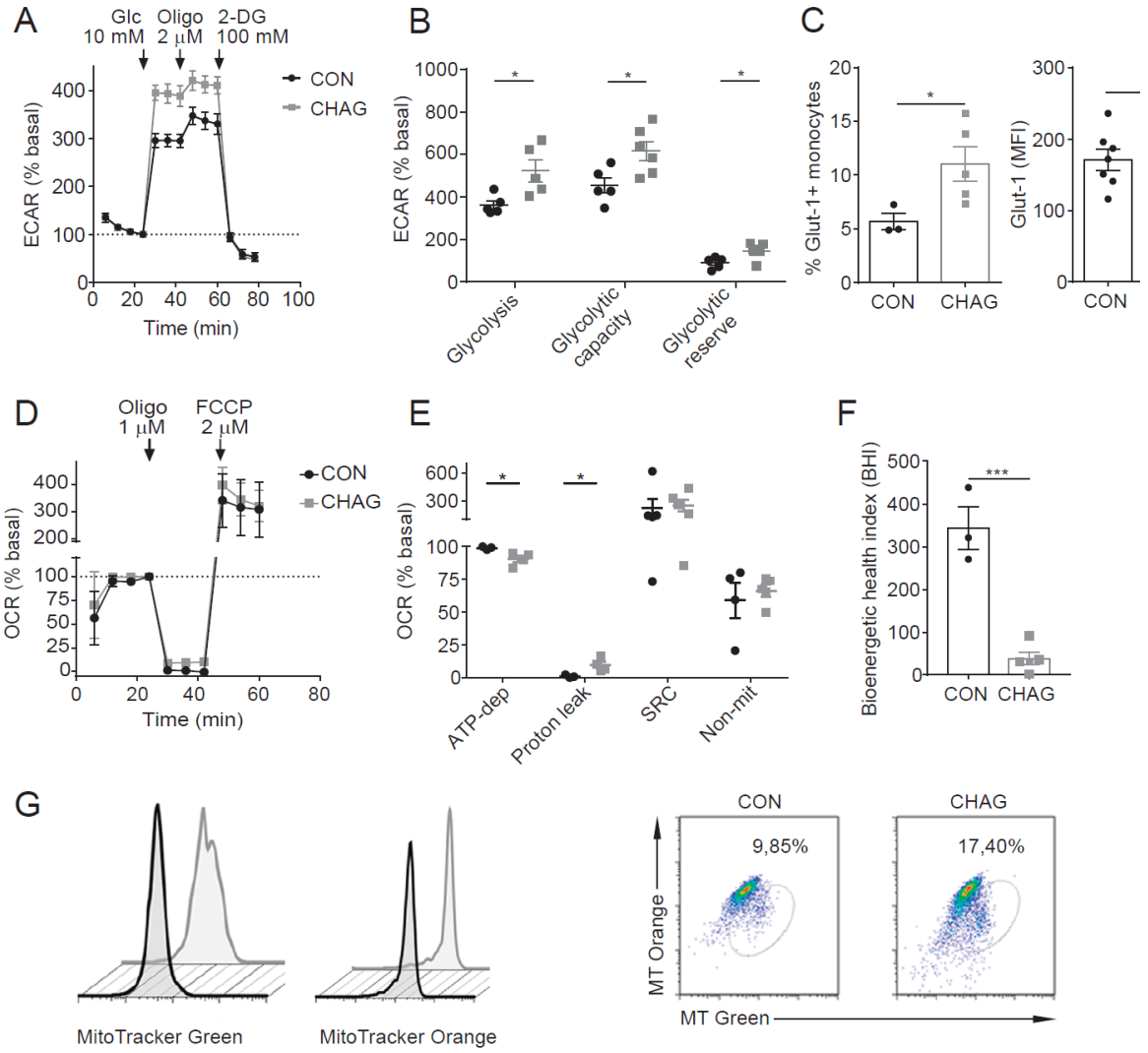

Figure 4: Monocytes from *T. cruzi*-infected patients show increased glycolysis and altered mitochondrial potential

(A) Monocytes from control donors (CON) or Chagas disease patients (CHAG) isolated by CD14 positive selection were seeded in a Seahorse XFp analyzer and real-time extracellular acidification rate (ECAR) was determined during sequential treatments with glucose, oligomycin (ATP-synthase inhibitor) and 2-deoxyglucose (2-DG) (glycolysis inhibitor). Data represent mean ± SEM of 8 runs. **(B)** Bars show glycolytic rate, glycolytic capacity and glycolytic reserve of monocytes from CON (n=5) and CHAG (n=5). To analyze these parameters first non-glycolytic acidification was subtracted, and then the data were normalized to basal ECAR. **(C)** Frequency and MFI of Glut-1+ monocytes from CON (n=3) and CHAG (n=5). **(D)** Real-time mitochondrial respiration was analyzed starting from basal respiration and after the addition of oligomycin (complex V inhibition), FCCP (maximal respiration induction), and rotenone/antimycin A mixture (electron transport chain inhibition). Data represent means ±SEM of 5 experiments. Bars show **(E)** respiration driving-ATP synthesis, respiration driving proton leak, spare respiratory capacity (SRC) and non-mitochondria OCR, and **(F)** bioenergetics health index (BHI) of monocytes from CON (n=4) and CHAG (n=5). To analyze these parameters first non-mitochondrial OCR was subtracted, and then the data were normalized to basal OCR. **(G)** Representative histogram of total mitochondrial mass analyzed by flow cytometry in monocytes from CON (black line) and CHAG (grey line) labeled with MitoTracker Green. Mitochondrial membrane potential (Δψm) was analyzed in monocytes from CON (black line) and CHAG (grey line) labeled with MitoTracker Orange. Representative dot plot of mitochondrial mass vs. mitochondrial

membrane potential in CON (n=3) and CHAG (n=5) monocytes. Data are presented as mean ± SEM. * $p < 0.05$, *** $p < 0.001$ (Student`s t test or Mann-Whitney test).

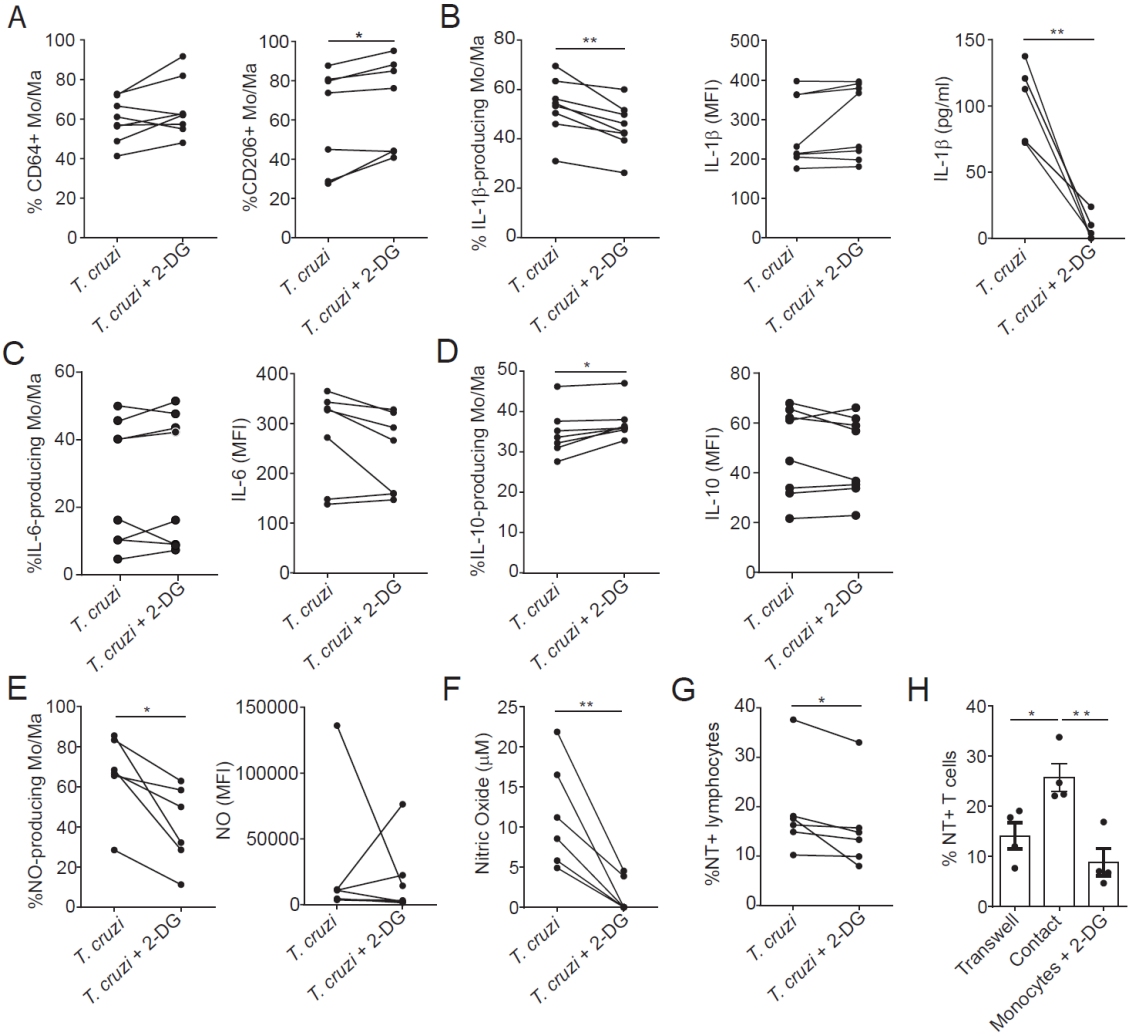

Figure 5: Glycolytic activity inhibition decrease NO-producing monocytes and lymphocyte nitration induced by *T. cruzi* infection

Infected PBMCs from control donors (8) were treated or not with 2-deoxyglucose (2-DG). **(A)** Frequency of CD64+ and CD206+ monocytes/macrophages (Mo/Ma). **(B)** Percentage and mean florescence intensity (MFI) of IL-1β+ Mo/Ma (left) and IL-1β levels in culture supernatants measured by ELISA (right). **(C)** Percentage and MFI of IL-6+, **(D)** IL-10+ and **(E)** NO+ Mo/Ma. **(F)** NO levels measured in culture supernatants by Griess reaction. **(G)** Frequency of TN^{+} CD3+ lymphocytes. * $p < 0.05$, ** $p < 0.01$ (paired Student`s t test or Wilcoxon test). **(H)** Infected purified monocytes from control donor (buffy coat) were cultured with purified lymphocytes in independent chambers (transwell) or in the same chamber (contact), in some co-cultures monocytes were treated with 2-DG (monocytes+2DG), (ANOVA with post-hoc Tukey) (representative experiment (n=4); from 2 independent experiments).

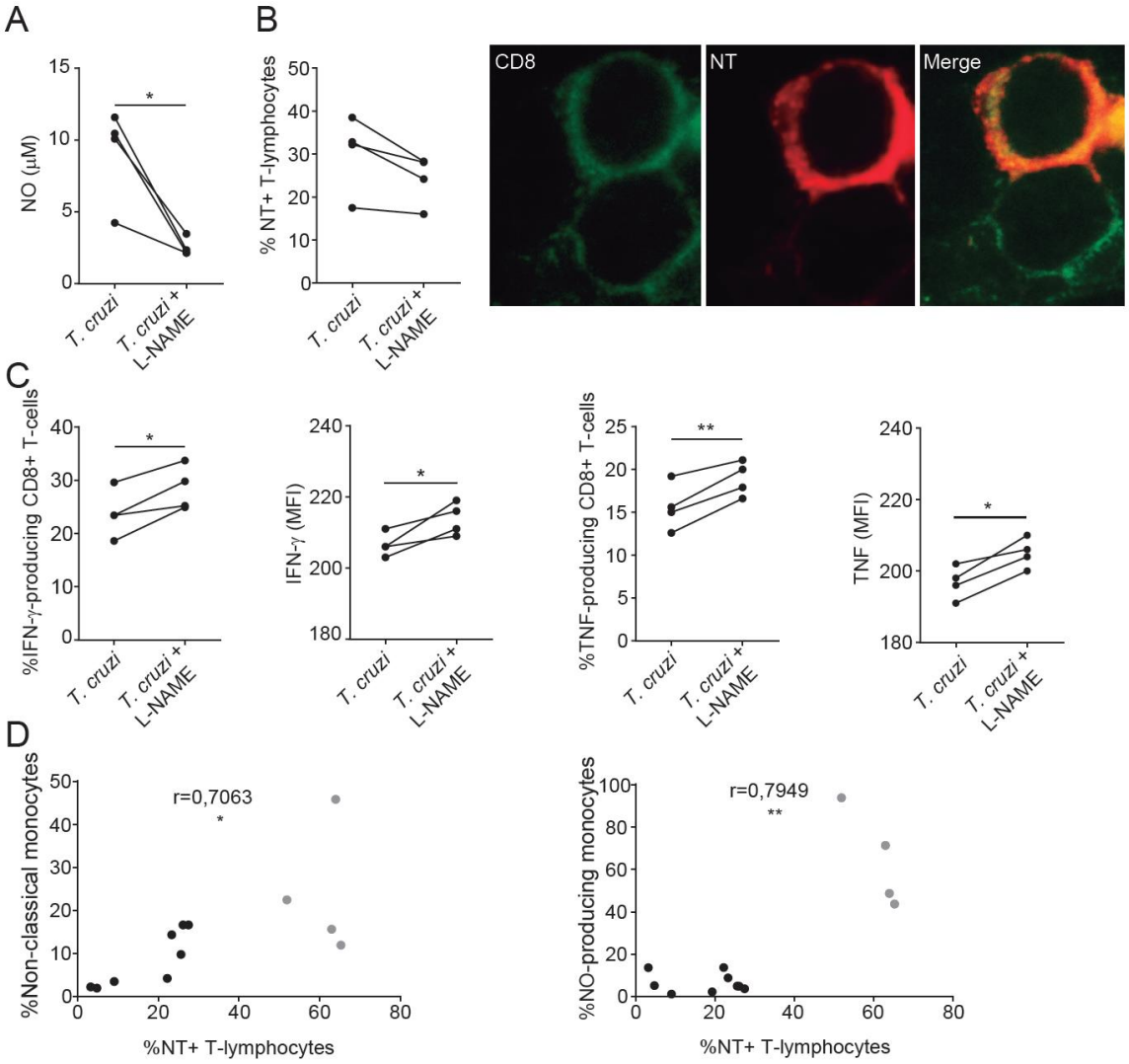

Figure 6: NO production drives tyrosine nitration on CTLs surface and CD8 T cell dysfunction

Infected PBMCs from control donors (4) were treated or not with L-NAME. **(A)** NO levels in culture supernatants measured by Griess reaction. **(B)** Frequency of TN^+ CD3+ lymphocytes (left) and representative images of cells from seropositive patient peripheral blood labeled with anti-TN antibody (red) and anti-CD8 antibody (green) (1000x) (right). **(C)** Percentage and mean fluorescence intensity (MFI) of IFN-γ+ and TNF+ cells also positive for CD8 and CD3 expression. * $p < 0.05$, ** $p < 0.01$ (paired Student`s t test or Wilcoxon test). **(D)** Pearson correlation analysis between the percentage of TN^+ CD3+ lymphocytes vs. the frequency of non-classical monocytes (left) and between the percentage of TN^+ CD3+ lymphocytes vs. the frequency of NO-producing monocytes (right) from control donors (black dots; n=8) and from seropositive patients (grey dots; n=4).

Table 1: Demographic and clinical data

	Control donors (CON) *n*=55	Chagas disease patients (CHAG) *n*=40
Age (years old)		
Range	19-60	20-60
Median	31	35
Gender		
Female	*n*=37	*n*=30
Male	*n*=18	*n*=10
Clinical evaluation		
Electrocardiographic changes	*NE*	*n*=5
Echocardiographic changes	*NE*	*n*=5
Chest X-rays abnormalities	*NE*	*n*=1

NE Not Evaluated